Quantum interference and manipulation of entanglement in silicon wire waveguide quantum circuits

2012 New J. Phys. 14 045003

(http://iopscience.iop.org/1367-2630/14/4/045003)

New Journal of Physics
The open-access journal for physics

Quantum interference and manipulation of entanglement in silicon wire waveguide quantum circuits

D Bonneau[1], E Engin[1], K Ohira[2], N Suzuki[2], H Yoshida[2], N Iizuka[2], M Ezaki[2], C M Natarajan[3], M G Tanner[3], R H Hadfield[3], S N Dorenbos[4], V Zwiller[4], J L O'Brien[1] and M G Thompson[1,5]

[1] Centre for Quantum Photonics, H H Wills Physics Laboratory and Department of Electrical and Electronic Engineering, University of Bristol, Merchant Venturers Building, Woodland Road, Bristol BS8 1UB, UK
[2] Corporate Research and Development Center, Toshiba Corporation, 1, Komukai Toshiba-cho, Saiwai-ku, Kawasaki 212-8582, Japan
[3] Scottish Universities Physics Alliance and School of Engineering and Physical Sciences, Heriot-Watt University, Edinburgh EH14 4AS, UK
[4] Kavli Institute of Nanoscience, TU Delft, 2628CJ Delft, The Netherlands
E-mail: mark.thompson@bristol.ac.uk

New Journal of Physics **14** (2012) 045003 (12pp)
Received 31 January 2012
Published 4 April 2012
Online at http://www.njp.org/
doi:10.1088/1367-2630/14/4/045003

Abstract. Integrated quantum photonic waveguide circuits are a promising approach to realizing future photonic quantum technologies. Here, we present an integrated photonic quantum technology platform utilizing the silicon-on-insulator material system, where quantum interference and the manipulation of quantum states of light are demonstrated in components orders of magnitude smaller than previous implementations. Two-photon quantum interference is presented in a multi-mode interference coupler, and the manipulation of entanglement is demonstrated in a Mach–Zehnder interferometer, opening the way to an all-silicon photonic quantum technology platform.

[5] Author to whom any correspondence should be addressed.

Contents

1. Introduction

Quantum information technologies offer completely new approaches to encoding, processing and transmitting information. By harnessing the properties of quantum mechanics, such as superposition and entanglement, it has been shown possible to realize fundamentally new modes of computation [1, 2], simulation [3, 4] and communication [5], as well as enhanced measurements and sensing [6]. Of the many prospective physical systems in which to encode quantum information, photons are a particularly promising approach owing to their properties of low noise, easy manipulation and low transmission losses. To date, quantum photonic integrated circuits have been realized in low-index-contrast waveguide material systems, such as silica [7, 8] and silicon oxy-nitride [9]. Such technologies offer benefits in terms of low propagation losses, but their associated large bend radii limits the scalability and usefulness of this technology.

Here, we present silicon quantum photonic waveguide circuits utilizing the silicon-on-insulator (SOI) material system, where quantum interference and the manipulation of quantum states of light were demonstrated in components orders of magnitude smaller than previous implementations. Quantum interference of indistinguishable photons was realized in multi-mode interference (MMI) couplers, and manipulation of multi-photon entanglement was demonstrated in a Mach–Zehnder interferometer (MZI).

2. Integrated quantum photonics

Traditionally, photonic quantum information experiments have been implemented using bulk optical elements, with photons propagating in free space. Although many proof-of-principle experiments have been reported, such an approach rapidly becomes impractical as the complexity of the quantum optical circuits increases, thereby making them inherently unscalable and confining them to research laboratory optical tables. In addition, sub-wavelength stability is critical for the reliable operation of many quantum circuits owing to the need for often complex networks of nested interferometers. However, developments over the last few years have overcome these bottlenecks through the implementation of integrated quantum circuits, allowing quantum information science experiments to be realized that are inherently

stable and orders of magnitude smaller than their equivalent bulk optic implementations. Integrated quantum photonic circuits have been demonstrated in a host of different material systems, including silica-on-silicon [8, 10], direct write silica [7, 11], silicon oxy-nitride [9], lithium niobate [12] and gallium nitride [13], all realized in low-index-contrast waveguide structures. Two-photon quantum interference has been reported in both silica and gallium nitride [10, 13], while manipulation of quantum states of light has been demonstrated using silica-on-silicon [8, 14] and lithium niobate [12], the later being also a promising material for photon pair generation [15]. The SOI wire waveguide technologies offer a further level of control, stability and miniaturization and also allow routes for on-chip generation and detection of photons. The high refractive index contrast provides compactness unrivalled by any other photonic material system, allowing a dramatic reduction in the footprint of quantum circuits and the integration of complex circuits on a single chip. Thermo-optic heaters, p–n junction modulators and induced χ^2 nonlinearities [16] allow for dynamically reconfigurable circuits with the possibility of fast phase control. The high third-order nonlinearity of silicon enables on-chip generation of quantum states of light via spontaneous four-wave mixing [17], thus allowing the integration of single-photon sources and waveguide circuits on the same chip. In recent years, high-efficiency on-chip single-photon detectors integrated with silicon waveguides have been reported [18]. Demonstration of quantum interference and manipulation of quantum states of light in a silicon waveguide circuit are the next critical step for realizing photonic quantum technologies in silicon. In this paper, we report on quantum interference and phase manipulation of one- and two-photon states using thermo-optic phase shifters and MMI devices on a silicon chip, opening up the way to a CMOS-compatible silicon-based photonic quantum technology platform where sources, detectors and circuits can all be realized monolithically on the same integrated chip for applications in communication, computing and metrology.

3. Experimental details

The silicon integrated waveguide circuits were fabricated from an SOI substrate with a silicon thickness of 220 nm. The single-mode optical waveguides had a width of 450 nm and a top cladding of silicon dioxide. Input and output coupling to lensed fiber was achieved using spot-size converters (SSC) comprising a 300 μm long inverse-taper with a 200 nm tip width and a $4 \times 4\ \mu m^2$ polymer waveguide. The silicon waveguiding structures were defined by 248 nm lithography and formed by dry etch processing. Typical propagation losses of 3.5 dB cm^{-1} and SSC losses of 2 dB per facet were observed, leading to device losses in the range of 6–10 dB. To realize the beam-splitter-like operation required for quantum interference, a 2×2 MMI coupler was designed (using finite-difference time-domain (FDTD) simulations) and implemented with dimensions of $2.8\ \mu m \times 27\ \mu m$ and input tapers of length 3 μm and width 1 μm (figure 1(a)). MZIs were formed from two MMI couplers and a 200 μm long thermo-optic phase shifter, shown in figure 1(b). By varying the voltage across the phase shifter it was possible to tune the internal phase delay of the MZI. Pairs of indistinguishable single photons at a wavelength of 1550 nm were generated from a type-I spontaneous parametric down conversion source (SPDC). A bismuth borate BiB_3O_6 (BiBO) nonlinear crystal was pumped by a 775 nm, 150 fs pulsed Ti-sapphire laser, and degenerate photon pairs were collected from two diametrically opposite points on the SPDC cone using single-mode fibers, and coupled into the chip using lensed fibers. One arm of the collection system was on a motorized delay stage to provide a tunable delay between the photon pair. The 1550 nm photons were coupled out of the chip using single-mode

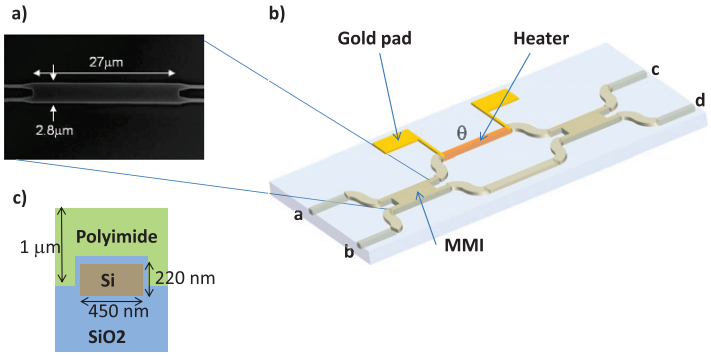

Figure 1. MMI and MZI. (a) SEM image of an MMI device. (b) Schematic diagram of a waveguide circuit with a voltage-controlled phase shifter. (c) Illustration of the cross-section of the single-mode waveguide.

lensed fiber and detected using two superconducting single-photon detectors (SSPDs), having system detector efficiencies of 5 and 15% [19, 20]. Coincidence detection between the two output ports of the device was performed using a custom made (field-programmable gate array (FPGA)-based) counting logic with a 5 ns coincidence window.

4. Quantum interference in a 2 × 2 multi-mode interference coupler

Quantum interference lies at the heart of linear quantum photonics and is fundamental to the implementation of any photonic quantum technology, describing at its most basic level the interaction of indistinguishable photons incident at a beamsplitter. In the case of two identical photons, each entering separate ports of a 50 : 50 beamsplitter device, the amplitude probabilities of both photons exiting different ports are zero—giving a superposition state of either both photons exiting one output port or both photons exiting the other output port. This quantum interference occurs for any physical implementation of a two-port beamsplitter device, and for an integrated waveguide circuit two typical implementations are the directional coupler and the MMI coupler.

MMI devices are based on the self-imaging principle, and when compared with directional couplers they have improved tolerances to fabrication and a wider spectral bandwidth of operation and can be extended to realize $N \times N$ multi-port devices with several input and output ports [21]. To demonstrate quantum operation of the SOI 2 × 2 MMI coupler, indistinguishable photon pairs were launched into each of the two input waveguides. At the two output ports, the two-photon coincidence counts were monitored. By varying the temporal delay between the two input photons, the indistinguishability of the input state could be controlled and the Hong–Ou–Mandel (HOM) dip [22] could be observed (see the inset of figure 3). A maximum dip raw visibility of $80 \pm 3\%$ was observed, demonstrating quantum interference.

A limited visibility of 80% was achieved in part due to multi-photon events generated by the pulsed source, in part due to intrinsic losses within the MMI device and also due to residual distinguishability of the generated photon pairs. The indistinguishability of the SPDC-generated photon pairs was characterized by performing a HOM experiment with a bulk-optic beamsplitter, giving a maximum visibility of $95.5 \pm 1.5\%$ for low pump power. Due to the chip insertion losses (a total of 9 dB including input/output coupling) and detector efficiencies (5 and 15%), it was necessary to pump the SPDC source in a regime where high count rates

could be achieved, which gave rise to multi-photon events that reduced the raw visibility of the dip. In order to quantify the effect of these multi-photon events, the raw visibility at different pump powers was measured (see figure 3), clearly demonstrating improved visibility for reduced photon pairs per pulse. By fitting to a model that accounts for multi-pair generation and system losses (see the appendix), an extrapolated nominal visibility of $88 \pm 3\%$ at low pump power was demonstrated.

The 7.5% discrepancy between the measured beamsplitter visibility of $95.5 \pm 1.5\%$ and the nominal MMI visibility of $88 \pm 3\%$ can be accounted for by the intrinsic losses within the MMI device. These losses do not enforce a $\varphi = \pi$ phase shift between the probability amplitudes for both the photons being reflected and both the photons being transmitted. A perfectly balanced 2×2 MMI should operate in exactly the same way as a perfect beamsplitter with the following scattering matrix:

$$\frac{1}{\sqrt{2}}\begin{bmatrix} 1 & 1 \\ 1 & -1 \end{bmatrix} = \frac{1}{\sqrt{2}}\begin{bmatrix} 1 & 1 \\ 1 & \mathrm{e}^{\mathrm{i}\pi} \end{bmatrix}. \tag{1}$$

In the presence of losses, we account for the loss modes by embedding the scattering matrix of the MMI in a larger 4×4 unitary transfer matrix written as

$$\begin{bmatrix} (\eta\overline{\alpha})^{\frac{1}{2}} & (\overline{\eta\alpha})^{\frac{1}{2}} & (\eta\alpha)^{\frac{1}{2}} & (\overline{\eta}\alpha)^{\frac{1}{2}} \\ (\overline{\eta\alpha})^{\frac{1}{2}} & \mathrm{e}^{\mathrm{i}\varphi}\,(\eta\overline{\alpha})^{\frac{1}{2}} & \mathrm{e}^{\mathrm{i}\theta}\,(\overline{\eta}\alpha)^{\frac{1}{2}} & \mathrm{e}^{\mathrm{i}\beta}\,(\eta\alpha)^{\frac{1}{2}} \\ (\eta\alpha)^{\frac{1}{2}} & \mathrm{e}^{\mathrm{i}\theta}\,(\overline{\eta}\alpha)^{\frac{1}{2}} & \cdots & \cdots \\ (\overline{\eta}\alpha)^{\frac{1}{2}} & \mathrm{e}^{\mathrm{i}\beta}\,(\eta\alpha)^{\frac{1}{2}} & \cdots & \cdots \end{bmatrix}, \tag{2}$$

where the upper left 2×2 sub-matrix represents the transfer matrix from the two input channels to the two output channels of the MMI, and the last two modes are losses. $0 \leqslant \eta \leqslant 1$ is the reflectivity of the MMI, $0 \leqslant \alpha \leqslant 1$ is the loss parameter, $\overline{\eta} = 1 - \eta$, $\overline{\alpha} = 1 - \alpha$, φ is the internal phase of the MMI and θ and β are the phases of the loss modes. Consequently, the phase between the probability amplitude for both photons being reflected and both photons being transmitted is not necessarily π anymore. The unitary condition gives a boundary on the internal phase φ as a function of the loss α:

$$\left|\cos\left(\frac{\varphi}{2}\right)\right| \leqslant \frac{\alpha}{1-\alpha}. \tag{3}$$

The nominal visibility of 88% is obtained using a source exhibiting a residual distinguishability, with a measured visibility of 95.5% obtained with a bulk beamsplitter. Assuming a perfect photon pair source (with ideal indistinguishable photons) the MMI visibility would be 92%. This non-unit visibility can be explained by an intrinsic MMI loss of 0.8 dB or greater (where figure 2 shows the lower bound on the MMI visibility) and yields an internal phase shift of $\varphi = 2.74$ instead of π phase shift. Indeed, FDTD simulations predict an intrinsic device loss of 0.5 dB, which is within the experimental error of the 0.8 dB calculated by the model. By reducing the intrinsic loss of the MMI to 0.2 dB (through improved device design and fabrication), the lower bound on the visibility would improve to 99.5%. It is worth mentioning that mode propagation simulation shows that the distortion of the single-photon wavepacket ($\sim$100 μm coherence length in free space) is insignificant in this experiment and does not contribute to a reduction of the visibility.

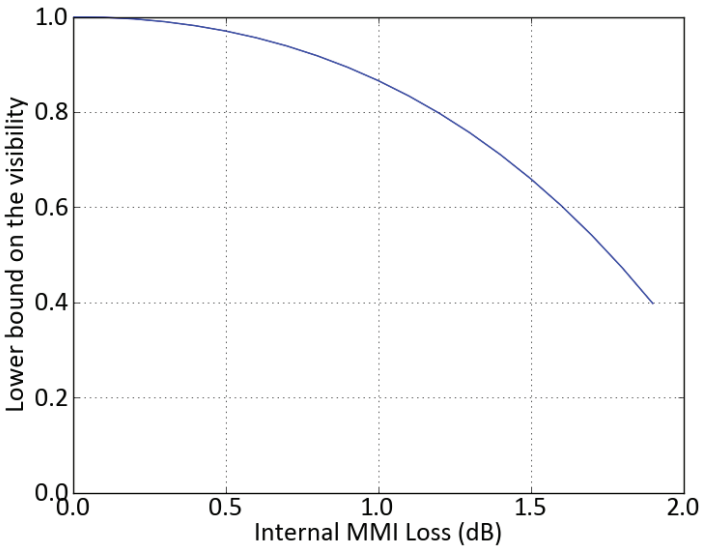

Figure 2. Lower bound on the visibility as a function of the MMI internal loss. This graph shows how the lower bound on the visibility of a HOM dip, performed on an MMI with perfect single-photon sources, evolves as a function of the MMI internal losses.

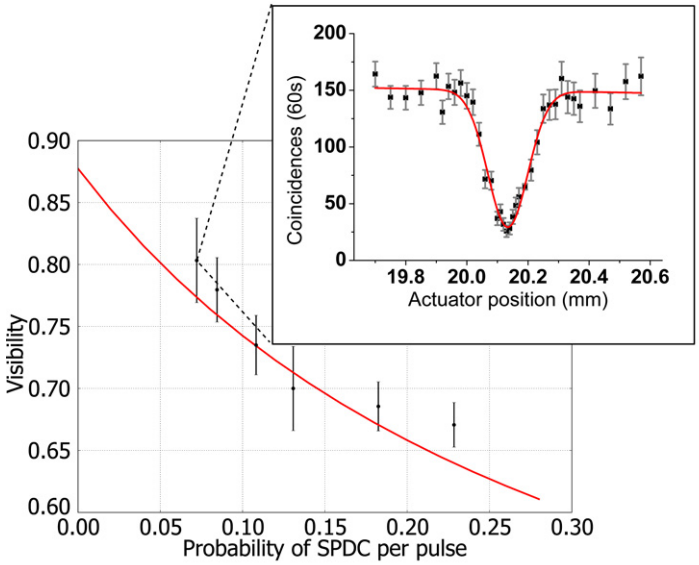

Figure 3. Visibility as a function of the probability of obtaining a photon pair. Visibility of the HOM experiment is plotted as a function of the probability per pulse of generating a photon pair. The solid line is a theoretical fit using a model that accounts for multi-photon events and losses before and after the MMI. The inset shows the two-photon interference plot for the highest visibility measurement.

5. Two-photon entangled state manipulation

The ability to actively prepare and measure arbitrary quantum states is crucial for the implementation of many quantum information processing experiments. Manipulation of dual rail-encoded qubits—a single photon in an arbitrary superposition of two optical channels—requires the control of the relative phase and amplitude between the two optical paths. Arbitrary single-qubit operations can be implemented using just two Hadamard gates (beamsplitter) and phase shifters, with the simple MZI considered to be the most basic fundamental building block required to realize any arbitary N-mode linear quantum photonic circuit [23].

To demonstrate the operation of this fundamental building block, an SOI MZI was formed from two 2×2 MMI couplers and a thermo-optic phase shifter (see figure 1(b)). The MZI on its own can apply only a subset of single-qubit operations, but any arbitrary single-qubit operation can be achieved by simply adding another phase-shifter element before and after the MZI [14]. This device was characterized in both the single-photon and two-photon regimes.

In the first instance, single photons were input into port a (see figure 1(b)), and as the internal phase of the MZI was changed, by applying a voltage across the thermo-optic phase shifter, the probability of detecting photons at the output port c varied sinusoidally as $P_c = \frac{1}{2}[1 - \cos(\phi)]$, with a periodicity of 2π. The observation of this classical interference fringe represents the ability to transform a single-photon input in mode a into a superposition state across modes c and d, given by the transformation $|10\rangle \rightarrow \cos(\phi/2)\,|10\rangle + \sin(\phi/2)\,|01\rangle$, where ϕ represents the phase shift within the interferometer. In the second instance, the two-photon $|11\rangle$ state was used, with one photon injected into port a and the other into port b. This input state leads to quantum interference at the first MMI couplers and, after propagating through the phase shifter, transforms to the two-photon entangled state $\frac{1}{\sqrt{2}}(|2\rangle\,|0\rangle + \exp^{2i\phi}\,|0\rangle\,|2\rangle)$. Quantum interference at the second MMI coupler enables the analysis of this quantum state, giving the probability output of coincidence detections $P_{c-d} = \frac{1}{2}[1 - \cos(2\phi)]$, with a periodicity π-half that of the single-photon case.

The measured single-photon and two-photon fringes are shown in figure 4 for an applied voltage change from 0 to 4.5 V, resolving 1.5 fringes for the single-photon case, and 3 fringes for the two-photon case. The two-photon fringe had a raw visibility of $V = 81.8 \pm 1.3\%$, which is greater than the threshold $V_{\text{th}} = 1/\sqrt{2}$ required to beat the standard quantum limit, demonstrating quantum metrology and the ability to achieve sub-shot noise-limited measurement.

6. Discussion

This work is the first demonstration of the interference and manipulation of quantum states of light in silicon integrated quantum circuits, and is a fundamental step toward further miniaturization of photonic quantum circuits. All previous integrated waveguide quantum circuits have relied on weakly guided waveguide structures, with a typical index contrast for the silica-on-silicon waveguide technologies of 0.5%, resulting in a bend radius of greater than 10 mm [14]. This low-index contrast and large bend radius result in physically large circuits and components, making future implementations of complex quantum circuit architectures impractical. Due to the high index contrast of the SOI material systems, it is possible to achieve bend radii of below 10 μm—three orders of magnitude smaller than the silica material system.

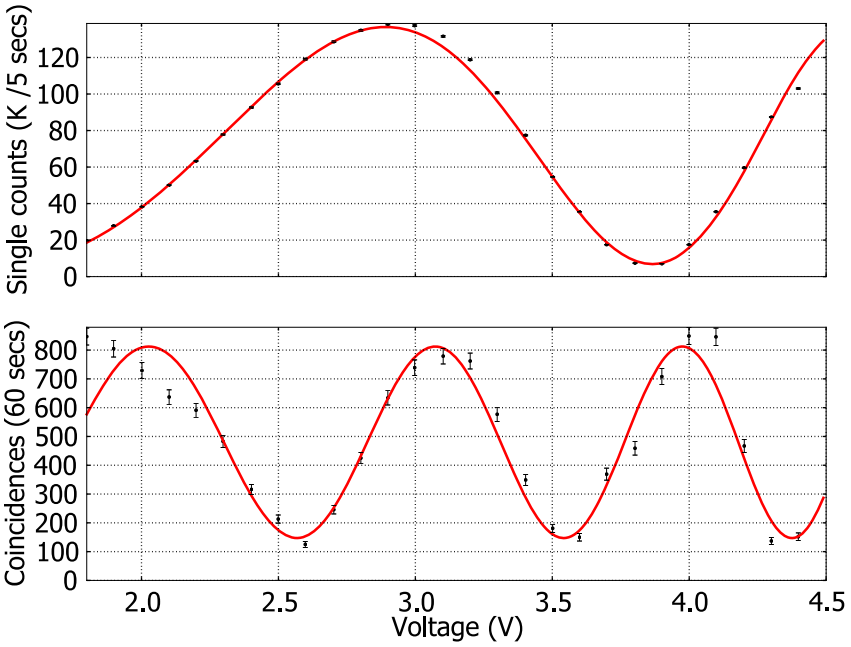

Figure 4. Single-photon and two-photon fringes. (a) Single-photon count rate as a function of voltage applied to the thermo-optic phase-shifter for the input state $|10\rangle$. (b) Two-photon coincidence count rate as a function of applied voltage for the input state $|11\rangle$. The x-axis represents the applied voltage across the thermo-optic phase shifter. The top figure shows the single-photon fringe. The y-axis represents the number of single photons recorded at one output of the MZI. The bottom figure shows the two-photon fringe. The y-axis represents the number of coincidence counts obtained for the two-photon fringe.

Individual components can be dramatically reduced in size, such as the 2×2 MMI coupler presented here that is 40 times smaller in length (27 μm) compared to the 1.1 mm length of the equivalent device in silica [24]. This enables circuits of significantly greater complexity to be realized while still maintaining a small chip size, but potentially at the cost of higher waveguide losses.

The key functions required to realize a fully integrated linear-optic quantum technology are the generation, detection, interference and manipulation of quantum states of light, all on a single optical on-chip. The generation and detection of single-photon states in silicon wire waveguide devices have been demonstrated previously [17, 18], and in this paper we demonstrate the feasibility of on-chip interference and manipulation of quantum states of light in silicon wire waveguide circuits. The high χ^3 nonlinearity of silicon and the high modal confinement of the silicon wire waveguide enable efficient photon pair generation via spontaneous four-wave mixing, with a recent demonstration showing indistinguishable photon pair generation from two independent silicon wire waveguides with an external HOM dip visibility of 73% [25]. High-efficiency detection of single photons has also recently been demonstrated in silicon wire waveguide incorporating superconducting nanowire detectors, with an internal detector efficiency of 94% [18]. These recent demonstrations along with the study presented here represent the basic building blocks required to realize an integrated photonic

quantum technology platform where quantum states can be generated, manipulated, interfered and detected all on the same circuits, opening up new possibilities in quantum information science and applications. Ultimately this CMOS compatible technology could be integrated with conventional microelectronic circuits, providing on-chip driver circuits and fast logic.

7. Conclusion

Quantum interference and manipulation of quantum states of light in silicon wire waveguide circuits has been demonstrated in this paper. A maximum HOM dip visibility of $80 \pm 3\%$ was observed for a 2×2 MMI coupler, and a nominal visibility in the absence of multi-photon terms of $88 \pm 3\%$ was calculated. Internal MMI losses were shown to be the dominant mechanism for the reduced nominal visibility. An integrated MZI with a thermal phase shifter demonstrated on-chip entangled state manipulation with a two-photon fringe visibility of $81.8 \pm 1.3\%$. These results pave the way for the realization of fully integrated photonic quantum technologies in silicon.

Acknowledgments

This work was supported by EPSRC, ERC, the Centre for Nanoscience and Quantum Information (NSQI) and the European FP7 projects QUANTIP and PHORBITECH. MGT acknowledges support from the Toshiba Research Fellowship scheme. JLO'B acknowledges a Royal Society Wolfson Merit Award. RHH acknowledges a Royal Society University Research Fellowship. We thank Alberto Politi for useful discussions.

Appendix

This appendix describes the details of the model used to give the fit in figure 3.

A.1. Multiphoton treatment of quantum interference

The state produced by the SPDC source is assumed to be a non-degenerate squeezed state and can be written as

$$|\Psi\rangle = \sqrt{1-\xi^2} \sum_{n=0}^{\infty} \xi^n \, |n\rangle \, |n\rangle \tag{A.1}$$

with $0 \leqslant \xi < 1$, where ξ is the squeezing parameter, n is the number of photon pairs generated and $|n\rangle\,|n\rangle$ is the number of photons in the two spatial modes of the source. We label as P_{C1}, P_{C2} and P_{CC} the probabilities of detecting per pulse, respectively, a single photon at detector 1, a single photon at detector 2 and a coincidental event between the two detectors C1 and C2.

Those probabilities can be expressed as

$$P_{C1} = \sqrt{(1-\xi^2)} \sum_{n=1}^{\infty} \xi^{2n} \left(1 - (1-\eta_1)^n\right), \tag{A.2}$$

$$P_{C2} = \sqrt{(1-\xi^2)} \sum_{n=1}^{\infty} \xi^{2n} \left(1 - (1-\eta_2)^n\right), \tag{A.3}$$

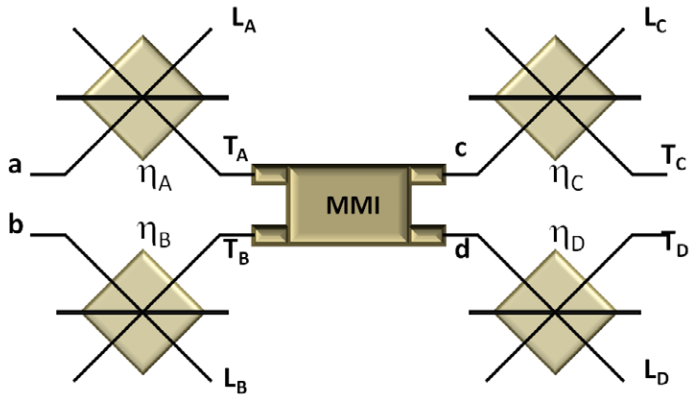

Figure A.1. Input and output losses modeling of a 2×2 MMI coupler.

$$P_{\mathrm{CC}} = \sqrt{(1-\xi^2)} \sum_{n=1}^{\infty} \xi^{2n} \left(1-(1-\eta_1)^n\right)\left(1-(1-\eta_2)^n\right) \tag{A.4}$$

with η_1 and η_2 being the overall efficiencies (including collection, transmission and detection) of, respectively, channels 1 and 2.

We measured the quantities C1 (the number of detection events per second at detector 1), C2 (the number of detection events per second at detector 2) and CC (the number of coincidental detection events per second at detectors 1 and 2) for different pump powers.

From those datasets, we ran minimization methods to relate the different count rates $C1$, $C2$, CC obtained from pump powers I_k to channel efficiencies η_1 and η_2 and the $\xi^2(I_k)$ parameter using the following equations:

$$C1(I) = f \times P_{C1}(I), \tag{A.5}$$

$$C2(I) = f \times P_{C2}(I), \tag{A.6}$$

$$CC(I) = f \times P_{CC}(I), \tag{A.7}$$

where $f = 80\,\mathrm{MHz}$ is the repetition rate of the pulsed laser and I is the intensity of the pump.

We then launched the state $|\Psi\rangle$ for different pump powers into the MMI coupler, and recorded quantum interference patterns with visibilities $V(I)$. In order to infer the visibility at low intensity, we applied the model described below.

A.2. Theoretical visibility

The theoretical visibility is expressed as $1 - \frac{P_{\mathrm{I}}}{P_{\mathrm{D}}}$, where P_{I} is the probability of getting a coincidental event when the photons generated in the two modes are indistinguishable, and P_{D} is the probability of getting a coincidental event when the two photons are distinguishable. If we used a true single-photon source in an ideal lossless circuit, $P_{\mathrm{I}} = 0$, $P_{\mathrm{D}} = 0.5$ and $V = 1$. However, we used a squeezed state $|\Psi\rangle$ as the input state, and the setup exhibits collection losses, propagation losses and non-unitary detection efficiencies. We modeled those losses by adding a virtual beamsplitter at each input and output port of the MMI coupler with reflectivities η_A, η_B and η_C, η_D, as shown in figure A.1. We trace over the loss modes L_A, L_B, L_C, L_D. All that is needed is to compute P_{I} and P_{D} by taking into account these losses.

We start with a pure squeezed state with a density matrix $\hat{\rho} = |\Psi\rangle\langle\Psi|$; we first propagate the state through the two input beamsplitters and then trace over the loss modes L_A and L_B. We further propagate the obtained reduced density matrix through the MMI coupler, assuming a 50/50 splitting ratio. We finally propagate the output state through the last two loss beamsplitters and trace over the modes L_C and L_D.

By writing $\hat{\rho}_{I\text{out}}$ as the final density matrix, we compute the probability of getting a coincidence by calculating

$$P_{\mathrm{I}} = \sum_{n=1}^{\infty}\sum_{m=1}^{\infty} \langle n|\langle m|\,\hat{\rho}_{I\text{out}}\,|n\rangle\,|m\rangle\,. \tag{A.8}$$

We implemented an algorithm to compute this probability to an arbitrary precision and found that computing terms up to $n, m = 9$ was accurate for the different pump powers we used. Adding higher-order terms did not change significantly the results.

For the case when the photons are distinguishable, we start with $|\Psi_{\mathrm{dist}}\rangle$ defined below and assume that the photons are orthogonal. In practice, one arm is delayed with respect to the other and we consider the photons launched in mode a at time t_1 and the photons launched in mode b at time t_2, giving

$$|\Psi_{\mathrm{dist}}\rangle = \sqrt{1-\xi^2}\sum_{n=0}^{\infty}\xi^n\,|n\rangle_{t_1}\,|n\rangle_{t_2}\,. \tag{A.9}$$

Then, applying the same evolution as previously for the indistinguishable photon case, we compute the probability P_{D} of getting a coincidence when the photons are distinguishable.

A.3. Fit of the experimental data

We recorded the visibility as a function of the pump power. For each intensity, we compute the associated squeezing parameter (ξ). The collection and detector efficiencies and the device losses are known. The only free parameter over which we need to minimize is the visibility. We therefore use an equation of the form

$$V(\xi) = 1 - \frac{\alpha P_{\mathrm{I}}(\xi) + (1-\alpha)\,P_{\mathrm{D}}(\xi)}{P_{\mathrm{D}}(\xi)}, \tag{A.10}$$

where α is the parameter that quantifies the overlap between the photons that includes residual spectral entanglement from the source and imperfections in the MMI coupler. Using this model, we extrapolate the nominal visibility that would be expected at very low pump power.

References

[1] Nielsen M A and Chuang I L 2004 *Quantum Computation and Quantum Information* (*Cambridge Series on Information and the Natural Sciences*) 1st edn (Cambridge: Cambridge University Press) pp 1–59
[2] Deutsch D 1985 Quantum theory, the Church–Turing principle and the universal quantum computer *Proc. R. Soc.* A **400** 97–117
[3] Feynman R 1982 Simulating physics with computers *Int. J. Theor. Phys.* **21** 467–88
[4] Lloyd S 1996 Universal quantum simulators *Science* **273** 1073–8
[5] Gisin N and Thew R 2007 Quantum communication *Nature Photonics* **1** 165–71
[6] Giovannetti V, Lloyd S and Maccone L 2004 Quantum-enhanced measurements: beating the standard quantum limit *Science* **306** 1330–6

[7] Crespi A, Ramponi R, Osellame R, Linda Sansoni L, Irene Bongioanni I, Sciarrino F, Vallone G and Mataloni P 2011 Integrated photonic quantum gates for polarization qubits *Nature Commun.* **2** 566–71
[8] Shadbolt P J, Verde M R, Peruzzo A, Politi A, Laing A, Lobino M, Matthews J C F, Thompson M G and O'Brien J L 2012 Generating, manipulating and measuring entanglement and mixture with a reconfigurable photonic circuit *Nature Photonics* **6** 45–9
[9] Peruzzo A *et al* 2010 Quantum walks of correlated photons *Science* **329** 1500–3
[10] Politi A, Cryan M J, Rarity J G, Yu S and O'Brien J L 2008 Silica-on-silicon waveguide quantum circuits *Science* **320** 646–9
[11] Smith B J, Kundys D, Thomas-Peter N, Smith P G R and Walmsley I A 2009 Phase-controlled integrated photonic quantum circuits *Opt. Express* **17** 13516–25
[12] Bonneau D, Lobino M, Jiang P, Natarajan C M, Tanner M G, Hadfield R H, Dorenbos S N, Zwiller V, Thompson M G and O'Brien J L 2012 Fast path and polarisation manipulation of telecom wavelength single photons in lithium niobate waveguide devices *Phys. Rev. Lett.* **108** 053601
[13] Zhang Y, McKnight L, Engin E, Watson I M, Cryan M J, Gu E, Thompson M G, Calvez S, O'Brien J L and Dawson M D 2011 GaN directional couplers for integrated quantum photonics *Appl. Phys. Lett.* **99** 161119
[14] Matthews J C F, Politi A, Stefanov Andre and O'Brien J L 2009 Manipulation of multiphoton entanglement in waveguide quantum circuits *Nature Photonics* **3** 346–50
[15] Aboussouan P, Alibart O, Ostrowsky D B, Baldi P and Tanzilli S 2010 High-visibility two-photon interference at a telecom wavelength using picosecond-regime separated sources *Phys. Rev.* A **81** 021801
[16] Jacobsen R S *et al* 2006 Strained silicon as a new electro-optic material *Nature* **441** 199–202
[17] Sharping J E, Lee K F, Foster M A, Turner A C, Schmidt B S, Lipson M, Gaeta A L and Kumar P 2006 Generation of correlated photons in nanoscale silicon waveguides *Opt. Express* **14** 12388–93
[18] Pernice W, Schuck C, Minaeva O, Li M, Goltsman G N, Sergienko A V and Tang H X 2011 High speed travelling wave single-photon detectors with near-unity quantum efficiency arXiv:1108.5299
[19] Tanner M G *et al* 2010 Enhanced telecom wavelength single-photon detection with NbTiN superconducting nanowires on oxidized silicon *Appl. Phys. Lett.* **96** 221109
[20] Dorenbos S N, Reiger E M, Perinetti U, Zwiller V, Zijlstra T and Klapwijk T M 2008 Low noise superconducting single photon detectors on silicon *Appl. Phys. Lett.* **93** 131101
[21] Soldano L B and Pennings E C M 1995 Optical multi-mode interference devices based on self-imaging: principles and applications *J. Lightwave Technol.* **13** 615–27
[22] Hong C K, Ou Z Y and Mandel L 1987 Measurement of subpicosecond time intervals between two photons by interference *Phys. Rev. Lett.* **59** 2044–6
[23] Reck M, Zeilinger A, Bernstein H J and Bertani P 1994 Experimental realization of any discrete unitary operator *Phys. Rev. Lett.* **73** 58–61
[24] Peruzzo A, Laing A, Politi A, Rudolph T and O'Brien J L 2011 Multimode quantum interference of photons in multiport integrated devices *Nature Commun.* **2** 224
[25] Harada K-I, Takesue H, Fukuda H, Tsuchizawa T, Watanabe T, Yamada K, Tokura Y and Itabashi S-I 2011 Indistinguishable photon pair generation using two independent silicon wire waveguides *New J. Phys.* **13** 065005